OCCURRENCE OF SPRINGS IN MASSIFS OF CRYSTALLINE ROCKS, NORTHERN PORTUGAL

FERNANDO ANTÓNIO LEAL PACHECO

fpacheco@utad.pt

ANA MARIA PIRES ALENCOÃO

alencoao@utad.pt

Department of Geology

Trás-os-Montes e Alto Douro University

5000 Vila Real

Portugal

Fax: (351) (259) 350480

ABSTRACT

An inventory artesian springs blooming from fractures (fracture springs) was conducted in the Pinhão River Basin and Morais Massif, northern Portugal, comprising an area of approximately 650 km^2. Over 1,500 springs were identified and associated with geological domains and fracture sets. Using Cross-Tabulation Analysis, spring distributions by fracture sets were compared among geological environments, and the deviations related to differences in rock structure and, presumably, to differences in deformational histories. The relation between spring frequencies and rock structures was further investigated by Spectral Determination, the model introduced in this study. Input data are the spring frequencies and fracture lengths in each geological domain, in addition to the angles between fracture strikes and present-day stress-field orientation (θ). The model's output includes the so-called intrinsic densities, a parameter indexing spring occurrence to factors such as fracture type and associated deformational regime and age. The highest densities (12.2 springs/km of lineament) were associated with young shear fractures produced by brittle deformation, and the lowest (0.1) with old tensional and ductile fractures. Spectral Determination also relates each orientation class to a dominant structural parameter: where spring occurrence is controlled by θ, the class is parallel to the present-day stress-field orientation; where the control is attributed to the length of fractures, the spring occurrence follows the strike of large-scale normal faults crossing the region.

Number of words: 219.

KEYWORDS*: spring occurrence, fracture length and strike, present-day stress-field orientation, fracture type and age, deformational regime*

INTRODUCTION

The number of springs emerging from fractured crystalline rocks depends on several factors, including the climate (precipitation and evapotranspiration), geomorphology, lithology, fracture density and pattern, and the present-day intensity and orientation of the regional stress field. These factors interact, and in some cases we can only reach conclusions by making a combined analysis of all or at least part of them. For example, identical lithologies in different regions may show rather different spring densities, and the reason for this may be clarified by considering the fracture densities of each region and/or their rainfall averages and regimes.

Early studies on spring occurrence were conducted by Bryan (1919), who has divided springs into gravity and non-gravity springs, and classified the first ones into several general types: depression, contact, fracture-artesian, and solution-tubular springs. The classical analysis of Brady (1919) has been corroborated by authors such as Todd (1980), Davis and DeWiest (1991), Fedeli and Castillo (1997), Martín *et al*. (1997), Portugal Ferreira and Pacheco (1997), and others. In most of these works, advances in knowledge have been made relative to Brady's work: the focus has no longer been put on the classification (or simply the assignment) of gravity springs into types, but on the identification and analysis of factors controlling the distribution of similar types of springs. In this context, Fedeli and Castillo (1997) pointed out that in the Upper Dilar Valley (Sierra Nevada, Spain), no matter the type, about 70% of the springs occur between 2,600 and 2,800 m above sea level, in a surface area of just 30% of the valley's total area. Martín *et al*. (1997) concluded that the distribution of fracture-artesian springs in several granitic areas of Spain is conditioned mostly by topographic relief, the lowest spring densities being associated with flat areas and the highest with valleys of steep hillsides. Finally, in an area where Silurian metasediments crop out (Padrela mountain, northern Portugal), Portugal Ferreira and Pacheco (1997) noticed that fracture-artesian springs emerge preferably in quartzites (3.2 springs/km^2), then in phyllites (2.1), and finally in carbonaceous slates (1.1). They also observed that springs emerge mostly from young fractures (corresponding to Alpine azimuths), from those making a low angle with the present-day stress-field orientation, and from those produced by shear during fold development (diagonal fractures).

The purpose of this study was to make another advance in the technique of analyzing spring occurrence. To that end, one redirected the focus on one of the above-mentioned factors controlling spring distribution—rock structure—and tried to better understand how spring frequencies relate to parameters such as fracture length, the angles between fracture strikes and the stress-field orientation, and the origin, deformational regime and age of fractures. The approach involved comprises two mathematical methods: (1) Cross-Tabulation Analysis (e.g. Jobson 1991), and (2) a model introduced in this paper under the name Spectral Determination. The study area is comprised of the Pinhão River Basin and the Morais Massif, two regions in northern Portugal with distinct deformational histories, where detailed spring mapping has been conducted by Alencoão (1998) and Pacheco (2000).

GEOLOGICAL SETTING

The northwest segment of the Iberian peninsula (Figure 1) is characterized by the Hercynian emplacement of a pile of thrust sheets on top of autochthonous sequences, followed by the intrusion of granitic bodies. The Pinhão River Basin and the Morais Massif are parts of this segment: the Schist and Greywacke Complex (SGC) cropping out to the south of the Pinhão River Basin is a portion of the autochthon and the granites of the northern area are members of the late- and post-orogenic intrusions; the Morais Massif comprises two thrust-sheets, termed Ophiolitic Thrust Complex (OTC) and Upper Allochthonous Thrust Complex (UATC).

Sousa (1982) described the stratigraphy of the SGC, dividing it into six formations. In the Pinhão River Basin (area: 280 km^2; Figure 2a), most of the southern area is occupied by two of them, the Desejosa and Pinhão Formations. The first consists of dark banded schists, the second of hornfelses and greenish phyllites with greywacke lenses and disseminated magnetite. The Morais Massif (385 km^2, Figure 2b) is cut by a ENE-WSW fault (the Morais Fault) that separates a NW block, composed essentially of ophiolitic rocks (OTC) which are duplicated tectonically into the lower (OTC_A) and upper (OTC_B) ophiolites, from a SE block that comprises an ophiolitic unit overlain by a sequence of metamorphic rocks that has been interpreted to represent a section of continental crust (OTC+UATC). The ophiolitic rocks comprise most of the Morais Massif with, from top to bottom, amphibolites (oceanic basalts),

a sheeted dyke complex, flaser gabbros, and ultramafics (mostly serpentinized peridotites). The overlying metamorphic sequence comprises the Lagoa granitic augengneisses, that have been interpreted to represent a Precambrian basement, and the Lagoa micaschists, a flyschoid sequence containing microfossils of the Upper Cambrian to Lower Ordovician age (Ribeiro *et al*. 1990, Marques *et al*. 1992). The intrusions incorporate coarse- to fine-grained two-mica syn- to post-F3 granites, where F3 means the third phase of the Hercynian orogeny (Matos 1991).

Deformational Histories and Fracture Patterns

The structure of the SGC at the Pinhão River Basin is determined essentially by the first Hercynian deformation phase (F1, starting 379±12 million years ago). This phase originated NW–SE upright folds, although in some places the axial surfaces may assume anomalous directions, especially N–S and NE–SW. Second-phase (F2) upright folds are recognised in some sectors, with axial surfaces following the previous F1 trends (Pinto *et al*. 1987, Matos 1991, Diez Balda and Vegas 1992). Fracture patterns associated with the folds should in principle trend as follows: N40º–50ºW (longitudinal fractures), N40º–50ºE (cross fractures), N10º–20ºW and N70º–80ºE (conjugate pair of diagonal fractures). During the third phase (F3, 300±10 My), the granites intrude, and from that time on both the SGC and the granites undergo identical deformation. During the granite's emplacement, deformation is ductile, represented by N30º–60ºW and N60ºE–EW shear zones. After cooling, deformation becomes fragile, represented by late- and post-F3 faults trending in following directions: *late-F3 faults* - NS±10º and N30º–60ºE; *post-F3faults* - N10º–30ºE (Matos 1991; Pereira *et al*. 1993). Among post-F3 faults are two important large-scale structures, the Vila Real and Vilariça Faults, shown in Figure 1.

Deformation in the Morais Massif is more complex than that observed in the SGC or in the granites due to thrust-sheet emplacement. In the first phase, deformation reflects the W to E movement of the OTC on top of the Lower Allochthonous Thrust Complex (LATC, Figure 1) and the NNW to SSE movement of the UATC over the OTC. Near the thrust surfaces, the rocks were deformed by shear, with development of recumbent folds showing hinges orthogonal to the sense of those movements. Away from the thrust surfaces, the rocks were

deformed by buckling, with development of overturned folds showing NW–SE axial surfaces identical to those found in the SGC. During F2, the Morais Massif acquired its structure of a basin bounded by thrusts (Figures 1, 2b). Two sets of folds were produced: (1) a set of radial folds with hinges plunging to the center of that basin, and (2) a set of concentric and recumbent folds also plunging to the center of the basin. In the last phase, the basin just formed underwent a NW–SE compression, which induced the formation of upright folds with NE–SW axial planes. Syn- to post-tectonic faulting is characterized by the EW±10º, N40º–60ºW (syn), and NS–N30ºE (late to post) fracture families (Ribeiro 1974, Ribeiro *et al*. 1990, Marques *et al*. 1992, Marques *et al*. 1996). According to the previous description, the expected fracture patterns in the OTC and UATC should be as follows: *OTC* - Associated with the F1 folds, the sets of longitudinal, cross, and diagonal fractures should trend in the N50ºW, N40ºE, N10ºE, and N70ºE directions, when considering the body of the thrust sheet, and in the NS, EW, N60ºW, and N60ºE directions along the thrust surfaces. F2 produced "isotropic" folding, and associated with F3 should be found fold-related fractures trending in the N50ºE, N40ºW, N10ºW, and N70ºW directions; *UATC* - As in the previous situation, F1 folds are associated with the body of the thrust sheet and with thrust surfaces. The corresponding fracture sets should be oriented in the N60ºW, N30ºE, NS, N60ºE directions, in the body of the thrust sheet, and in the N80ºE, N10ºW, N40ºW, and N20ºE directions along the thrust surfaces. The last systematic set of fold-related fractures is originated by F3 and must include the N40ºE, N50ºW, N20ºW, and N80ºW directions.

Figure 3 shows the areal distribution of the lineaments and fracture traces, and rose diagrams of the lineament and fracture patterns, for the Pinhão River Basin and Morais Massif, interpreted from aerial photographs (scale: 1/25000) and the available geological information; as defined in Genter (1990), lineaments are linear or curvilinear discontinuities associated with morphological and/or tectonic features of the landscape. It is difficult to link the orientation classes (e.g. N10º-20ºE) from the rose diagrams to fracture types (e.g. fold-related fractures) observed in the field by the above-cited authors, because one class may represent different types. It is obvious however from the figures that the Morais Massif represents an environment that is more complex than the SGC or the granites. Indeed, while the number of peaks in the rose diagram of Figure 3a is restricted to three or four, probably enhancing the late and post-tectonic faulting imprinted by the granites' emplacement, in Figure 3b the

number of peaks increases to seven, probably showing that all deformational phases are represented significantly in the subsurface.

Stress Field

The stress pattern in the mainland of Portugal and adjacent Atlantic region was determined by Ribeiro *et al*. (1996) using three different approaches: geological stress indicators, borehole breakouts, and earthquake focal mechanisms. The analysis of the stress results suggests a progressive rotation of the direction of the maximum horizontal compression of the stress field (S_{Hmax}), from NNW–SSE in the Upper Pliocene to Middle Pleistocene (shown by the geological fault-slip data), to NW–SE in the Upper Pleistocene or Holocene (memorized in the upper crustal rocks and evidenced by the well-bore breakouts), and finally to a WNW–ESE trend in the present time (as indicated by the earthquake focal-mechanism data).

INVENTORY OF FRACTURE ARTESIAN SPRINGS

From April to October 1995, a number of springs (assumed fracture artesian) were mapped and associated with lithological domains (granites and SGC) and orientation classes (EW–N80ºW, N80º–70ºW, N70º–60ºW, N60º–50ºW,...., N60º–70ºE, N70º–80ºE, N80ºE–EW) in the Pinhão River Basin by Alencoão (1998). In the field, only the location of the springs was recorded, using 1/25000-scale topographic maps. The assignment of springs to lithological units or fracture-orientation classes was done by superposition of three maps, one with the identified springs and the other two with the lithological domains (Figure 2a) or the photo-interpreted lineaments and observed faults (Figure 3a). Basically, Alencoão (1998) decided that if a spring was located within the outcrop area of a certain lithological unit or over a particular lineament/fault, the two could be attached accordingly. In the latter case, the selected orientation class was based on the lineament's direction. When, in Figure 3a, a spring was close to but not exactly over a lineament/fault, or else was in the intersection between lineaments/faults, the spring was still considered to be fracture artesian, but no orientation class was attributed to it.

From August 1997 to October 1997 and August 1998 to October 1998, Pacheco (2000) conducted a spring inventory in the Morais Massif. Topographic maps at the 1/25000 scale were used to plot spring locations and superposition of maps was used to associate springs and lithological units (amphibolites and ultramafics within the OTC, Lagoa augengneisses and Lagoa micaschists within the UATC). Field criteria were used to link springs to specific orientation classes, which included: (1) direct observation of water emerging from a fracture (in only 2% of the cases). As with the method of Alencoão (1998), the selected orientation class was based on the fracture strike; (2) indirect criteria. In the vast majority of cases, springs emerge from fractures which cannot be seen linearly. Rather, around or near the springs are alignments of rushes, oriented man-made galleries, or rectilinear patterns of streamlets, which were assumed as the directions of conductive fractures. Following the method of Alencoão (1998), when none of these criteria could be applied to a particular spring, it was still assumed to be fracture artesian but no orientation class was attributed to it.

In total, 1,537 springs were mapped by Alencoão (1998) and Pacheco (2000). Figure 4 shows how springs are distributed inside the Pinhão River Basin and Morais Massif. Apparently, granites show much higher spring densities than the metassediments (compare Figures 2a and 4a). Also, the southern block of the Morais Massif, the one that is "fractured" more intensively according to Figure 3b, shows much higher spring densities than the northern block (Figure 4b). Table 1 summarizes the information on outcrop area, total length of lineaments and fractures, number of springs, and spring densities (N_A: number of springs per square km of surface area; Nk: number of springs per km of lineament) in each lithological unit. It is striking that the N_A values vary considerably among similar units (SGC and Lagoa micaschists; granites and Lagoa augengneisses) whereas the Nk values are roughly similar (Nk = 0.6±0.1 springs/km of lineament) in all units. This may indicate that rock structure controls the occurrence of springs in both areas, suggesting that the assumption about mapped springs being of the fracture-artesian type is acceptable.

MATHEMATICAL METHODS

The relation between spring frequencies and rock structure was investigated by two methods, Cross-Tabulation Analysis and a method referred to as Spectral Determination. Cross-

Tabulation Analysis was used to verify if the spring distribution by fracture-orientation classes is dependent significantly on the geological environment. Using Spectral Determination, a mathematical relation was derived between spring frequencies and structural parameters such as fracture length, the angle between fracture strike and stress-field orientation, and some property of fractures based on indexing the occurrence of springs to genetic factors such as fracture type (tensional or shear), associated deformational regime (fragile or ductile), and age.

Input Data for the Mathematical Methods

Table 2 summarizes the information used as input data for Cross-Tabulation Analysis and Spectral Determination. Spring frequencies and lineament/fracture lengths are depicted per major geological domain (granites, SGC, OTC, and UATC) and fracture-orientation class. Major geological domains replaced the lithological units in Table 1, because the former are characterized by different deformational histories and rock structures. Counts of springs to which no orientation class has been attached are indicated in Table 2 by the term N.A.. For the sake of maintaining data quality, these set of springs were omitted from the data analysis. By discarding the N.A. category of springs, it was assumed that the others are a random sample representing the whole population.

Cross-Tabulation Analysis

The method of Cross-Tabulation Analysis (e.g., Jobson 1991) is used with categorical data. These data consist of counts (or frequencies), for example of people, places, or springs. Counts are executed once the object has been associated with qualitative features, or quantitative attributes summarized into categories. If the analysis is focused on the springs emerging from rocks in the study area, selected features or attributes may be the geological environments and orientation classes to which they were linked. Each count will match the number of springs associated simultaneously with an environment and a class, for example the springs attributed to fractures in granites oriented N30º–40ºE or those in the OTC linked to N80º–70ºW azimuths.

Data for Cross-Tabulation Analysis are accommodated conveniently in two-entry tables termed cross tables, of which the left block of columns of Table 2 is a typical example. This (or any other) cross table contains: (1) variables (X and Y). X is assigned to orientation class and Y to geological environment; (2) categories (m and p). The m categories of X are the 18 orientation classes (EW–N80ºW, N80º–70ºW, N70º–60ºW, N60º–50ºW,...., N60º–70ºE, N70º–80ºE, N80ºE–EW) and the p categories of Y the four geological domains (granites, SGC, OTC, and UATC); (3) central cells (n_{ij}), which register the number of events of X on its i^{th} category, taking into account the events of Y on its j^{th} category. For example, the number of springs in the OTC (3^{rd} category of Y) attributed to the orientation class N80º–70ºW (2^{nd} category of X) is $n_{23} = 30$; (4) marginal cells ($n_{i.}$ and $n_{.j}$). They register the number of events in each category of X or Y; for example, the springs emerging from fractures oriented N30º–40ºE ($n_{13.} = 109$), or those blooming from the granites ($n_{.1} = 696$); (5) cross cell (n). This is the total number of events (n = 1,537). The relation between cell types is given by:

$$n_{i.} = \sum_{j=1}^{p} n_{ij}; \quad n_{.j} = \sum_{i=1}^{m} n_{ij}; \quad n = \sum_{i=1}^{m} n_{i.} = \sum_{j=1}^{p} n_{.j} \tag{1}$$

The main purpose of Cross-Tabulation Analysis is to verify whether frequencies in the columns of a cross table are dependent (significantly different from each other) or independent (showing identical patterns). This is established by the following χ^2 test: columns are independent if

$$G^2 \leq \chi^2 \tag{2a}$$

where χ^2 is obtained from the chi-square table and G^2 given by:

$$G^2 = \sum_{i=1}^{m} \sum_{j=1}^{p} \frac{(n_{ij} - e_{ij})^2}{e_{ij}}$$

$$\text{with} \tag{2b}$$

$$e_{ij} = \frac{n_{i.} n_{.j}}{n} \text{ (expected frequency)}$$

and dependent otherwise. In case columns are dependent, differences between them are visualized conveniently in line-type plots where conditional probabilities (f_{ij}) defined as:

$$f_{ij} = \frac{n_{ij}}{n_{.j}} \tag{3}$$

are represented: in these plots, lines drawn for each column are coincident except for orientation classes where frequencies are markedly distinct.

Spectral Determination

As shown in Table 1, Nk values do not vary considerably among lithological units (they approach 0.6 springs/km of lineament in all units). In other words, when leaving a geological domain with N1 springs and L1 kilometers of fractures by entering a different geological domain characterized by N2 springs and L2 kilometers of fractures, the relation between N and L is apparently maintained (also if climatic and morphological conditions do not change dramatically):

$$\frac{N}{L} = Nk \text{ (conservative)} \tag{4}$$

If the spring distribution by fracture-orientation classes was isotropic, meaning that it would not depend on the fracture strikes, the following equality would also apply:

$$\frac{N_i}{L_i} = Nd_i \approx Nk \qquad (i = 1,..., m) \tag{5}$$

where subscript i represents an orientation class, m is the number of orientation classes, N_i the number of springs emerging from fractures of strike i, L_i the total length of fractures of strike i, and Nd_i the density of springs along strike i (directional density). But the Nd_i values are far

less conservative than the Nk values: according to data in Tables 1 and 2, the Nk range is 0.5–0.7 (amplitude 0.2) whereas the Nd_i range is 0.1–2.1 (amplitude 2.0).

The spread in the Nd_i values may be explained by several factors. One is the stress-field orientation, which is called a factor of extrinsic nature. In principle, fractures which are parallel to the direction of maximum horizontal compression (S_{Hmax}) should be more open and therefore more favorable to the occurrence of springs. Conversely, fractures which are orthogonal to the S_{Hmax} should be more closed, thus showing lower Nd_i values. From one extreme situation to the other, it is believed that the influence of the stress field on the directional density of springs is determined by the tangential component of the maximum horizontal compression ($\sigma_{Hmax}\cos\theta_i$, where σ_{Hmax} is the maximum horizontal compression and θ_i the angle between S_{Hmax} and the strike of fracture family i), more precisely by its directional term ($\cos\theta_i$), as the effect of σ_{Hmax} is distributed equally in all directions.

Apart from the extrinsic factor, one should consider factors of intrinsic nature, namely those regarding the types of fractures which comprise each orientation class (shear or tensional fractures), deformational regimes which have generated each fracture family (fragile or ductile), and fracture ages. For instance, one would expect that shear fractures are associated more often with the occurrence of springs than tensional fractures, because a mylonitized zone is associated commonly with the former, which may become enlarged and allow better water circulation. One would also expect that fractures resulting from fragile breakage would be more permeable than ductile fractures as, in principle, the former are associated with a higher loss of cohesion. Finally, it is more reasonable that young fractures show higher Nd_i values than old fractures, because young fractures had less time to become sealed. The influence of intrinsic factors on the directional density of springs may be synthesized in the form of a parameter which is referred to as the intrinsic density of springs (c_i). This parameter is hardly measurable, but may be evaluated indirectly if, in Equation 5, Nd_i is replaced by its extrinsic ($\cos\theta_i$) and intrinsic (c_i) contributors:

$$\frac{N_i}{L_i} = c_i \cos\theta_i \qquad (6)$$

Rearranging, we obtain:

$$\frac{N_i}{L_i \cos\theta_i} = c_i \tag{7a}$$

$$N_i = L_i c_i \cos\theta_i \tag{7b}$$

Intrinsic densities are calculated from Equation 7a once corresponding directional densities (N_i/L_i) and S_{Hmax} are known from spring mapping, aerial-photographic interpretation of lineaments, and stress-field studies such as those carried out by Ribeiro *et al*. (1996). Besides, Equation 7a provides the means for a formal definition of c_i. This is the number of springs per kilometer in a fracture family of strike i if the i^{th} orientation class was parallel to S_{Hmax} (i.e., c_i is the upper limit of the number of springs one would expect to find in one kilometer of a fracture family trending in i). Equation 7b expresses spring frequencies explicitly in terms of their bearing factors. Line-type plots of spring densities (directional or intrinsic) or frequencies versus the corresponding orientation classes are termed spectra (directional, intrinsic, or total), and the method by which the intrinsic spectrum of a specific geological domain is delineated once its directional spectrum is known is termed Spectral Determination.

Spectra Decomposition

The above-mentioned spectra may be given two generic names: combined, when spectra are dependent simultaneously on various parameters, or individual otherwise. The first generic name is appropriate for total and directional spectra, as they are functions of three (L_i, c_i, and $\cos\theta_i$) or two (c_i and $\cos\theta_i$) parameters, whereas the second generic name applies to the intrinsic spectrum, because it depends solely on c_i. The purpose of spectra decomposition is to separate combined spectra into two additional individual spectra, one related exclusively to fracture lengths and the other to the present-day stress-field orientation. The method is illustrated in Figure 5 and described in the following paragraphs.

The individual spectrum depending exclusively on fracture lengths is obtained from combined spectra. Indeed, if the total spectrum depends on L_i, c_i, and $\cos\theta_i$, and the directional spectrum on c_i and $\cos\theta_i$, the difference between both will depend just on L_i. However, this difference cannot be calculated directly because the N_i and N_i/L_i values are expressed on different scales. One convenient way to convert them into the same scale is by calculating their standard distributions using the following equation:

$$Z = \frac{X - \text{Mean}(X)}{\text{Standard Deviation}\,(X)} \tag{8}$$

where X represents a spectrum in current units and Z the same spectrum in standard units. Applying Equation 8 to the total and directional spectra, the fracture-length spectrum is obtained from the following equation:

$$ZFL = ZT - ZD \tag{9a}$$

where FL, T, and D mean fracture-length, total, and directional, respectively. By analogy with ZFL, the individual spectrum depending solely on the present-day stress-field orientation (ZSF) is obtained by difference between the directional and intrinsic spectra, both expressed in standard units (ZD and ZI):

$$ZSF = ZD - ZI \tag{9b}$$

It should be mentioned that, by proceeding from Equation 8 to 9b, it is assumed that the difference between two standardized spectra is independent of the target variable.

The meaning of ZSF and ZI spectra has already been addressed, although indirectly. The first spectrum relates high spring frequencies with fractures striking parallel to the S_{Hmax}, and the second with young fractures generated by shear during periods of brittle deformation. By analogy, ZFL must link high spring frequencies to orientation classes that show abnormally large fracture lengths. The reasons for fracture-length anomalies are not apparent unless, for example, the region is cut by large-scale normal faults. In such cases, among the fracture

systems related genetically to these faults, the most pervasive are parallel to the fault or at least have a similar strike, and consequently the fracture length along the strike of the fault is enhanced with respect to the lengths along other fracture-orientation classes.

Peak Matching

Standardized spring densities match the following statistical description: (1) Z distributions have zero mean and standard deviation equaling or approaching one, depending on whether Z is calculated by Equation 8 or Equations 9a,b; (2) the $Z > 1$ and $Z < -1$ frequencies include the positive and negative anomalies present in the population; (3) values in the range $-1 < Z < 1$ are referred to as regular or non-anomalous z-scores. In line-type plots of Z versus orientation class, positive anomalies are represented by major peaks, positive z-scores usually by minor peaks, and negative values (regular or anomalous) by depressions. The Peak-Matching Technique aims at relating major and minor peaks in the total spectrum ($ZT > 0$) with major peaks in the individual spectra ($ZFL > 1$ and/or $ZI > 1$ and/or $ZSF > 1$); in other words, on linking observed spring frequencies (N_i) to their most influencing structural parameters (L_i and/or c_i and/or $\cos\theta_i$).

The Peak-Matching Technique is a graphical method operating in three consecutive steps:

Step 1 - Defining the Plot Area - The plot area for peak matching is a $p \times m$ cell-rectangle, where p and m are the number of width- and height-cells, and match the number of geological domains and orientation classes in study.

Step 2 - Assigning Orientation Classes to Major Individual Spectra Peaks - The cell corresponding to orientation class i and geological domain j is filled with a pattern if $Z_{ij} > 1$ (major peak), where Z is an individual spectrum, or left blank otherwise. Different patterns are used to represent ZFL, ZI, and ZSF. It is uncommon that more than one individual spectrum have $Z_{ij} > 1$ for a given pair (i,j), but when such cases occur the highest Z value determines the filling pattern.

Step 3 - Comparing ZT Peaks with Major ZFL, ZI, and ZSF Peaks - Major and minor total spectra peaks are represented in the plot area by symbols, for example bullets and circles. The relation between ZT peaks and major individual spectra peaks is set in accordance with the following conditions: (1) the ZT peak falls in a filled cell. In

such cases, the spring occurrence in the associated geological domains and orientation classes is controlled by just one structural parameter. Accordingly, peaks are considered as the single-parameter type; (2) the ZT peak falls in a blank cell. In such cases, the spring occurrence is due to small contributions of all or part of the intervening structural parameters. Thus, peaks are considered as the multiple-parameter type; (3) no ZT peak is associated with a filled cell. This happens when an individual spectrum favors the occurrence of springs along a certain direction ($Z > 1$) but greater negative influences ($Z < 0$) are coming from the other individual spectra.

RESULTS AND DISCUSSION

Cross Tabulation

The procedure that was followed to set the dependence or independence between geological domains, regarding distribution of springs per fracture-orientation classes, used information shown in Table 2. Applying Equation 2b to these data, $G^2 = 232.3$. For 99.999% of probability and 51 degrees of freedom ($(m-1) \times (p-1)$), the critical value of χ^2 is 86.7. Because G^2 exceeds this value, the hypothesis of independence (Equation 2a) is rejected, meaning that the distribution of springs per fracture-orientation classes depends on the prevailing geological environment.

Total spectra drawn for the Pinhão River Basin (granites and SGC) are shown in Figure 6a; conditional probabilities (Equation 3) replaced frequencies so that spectra could be compared easily. In the granites, orientation classes with the highest spring frequencies follow the N60ºW, N10ºW, and N20º–40ºE directions, corresponding to ductile syn-F3 shear zones, ductile/fragile late-F3 faults, and fragile post-F3 faults. All orientation classes that are important hydrogeologically in the granites are also relevant in the SGC, although peaks are shifted systematically 10º–20º towards the east in the latter case. This shifting is striking. It seems that the syn- to post-F3 faulting activates previous structures, especially the longitudinal (N50ºW) and cross (N40ºE) fractures generated during the F1 and F2 phases,

instead of imprinting new directions favorable to spring occurrence. A fourth peak appears in the total spectrum of the SGC, trending in N80ºW. The occurrence of this peak has no clear explanation. It is assumed that, in some places, the anomalous NE–SW F1 folds, which produce N80ºW diagonal fractures if axial surfaces follow the N40ºE trend, may become important groundwater conductors.

Total spectra drawn for the Morais Massif (OTC and UATC) are shown in Figure 6b. In this case, patterns of spring distribution are substantially different, with major deviations occurring preferably along the N70ºW and NS–N10ºE directions (higher frequencies in the OTC) as well as along the N30ºE, N50ºE, and N70º–80ºE directions (higher frequencies in the UATC). Apparently, the UATC spring distribution has a characteristic mark imprinted by syn- and late to post-F3 faults of ENE–WSW and NE–SW trends (especially the Morais Fault, which corresponds to the northern limit of the UATC; Figure 1), whereas in the OTC this mark is acquired mostly during the F3 folding that has generated N70ºW diagonal fractures.

Spectral Determination

The results obtained with the method of Spectral Determination are shown in Table 3. The first two columns contain the orientation classes and the angles between these classes and the present-day stress-field orientation, here represented by the N75ºW direction. The next four blocks of columns show the intrinsic densities, calculated by Equation 7a, and the names of specific Hercynian fractures.

As shown in Table 3, an orientation class may in some cases represent more than one fracture family; for example, the N30ºE class in the UATC represents simultaneously F1 cross fractures and post-F3 faults. In the following discussion, it is assumed that intrinsic densities reflect the most recent deformational history of the orientation classes, i.e. that densities shall be assigned to the youngest fracture family represented by that class (the post-F3 faults in the example). In agreement with this assumption, the following statements apply: (1) the highest c_i values in Table 3 (4 to 12 springs/km) are linked to post-F3 N10º–20ºE faults (FF); (2) immediately below these very high values are the densities of late-F3 faults (DFF, with 0.4

$< c_i < 4.0$); (3) on the side of the lowest intrinsic densities ($0 < c_i < 1$) are all the F1 and most of the syn-F3 fractures (e.g. L, C); exceptions in the latter case are the diagonal fractures cutting the OCT and UATC (D and Da), which have c_i values in the range 1.1–2.6 springs/km, and some ductile faults (DF), that in rare cases (3 in 18) show c_i values greater than 1 but never as much as $c_i = 2$.

The intrinsic densities in Table 3 were assembled according to fracture types, deformational regimes, and fracture ages. Corresponding ranges of c_i values are shown in Table 4. In brief, tensional and old fractures have low c_i values, young fractures have high c_i values, and ductile-shear fractures have low to moderate c_i values. It should be noted that values in Table 4 are not universal, as they are expected to change considerably if, for example, local precipitation is too different from that occurring in this study area (1000 mm/year in the Pinhão River Basin and 720 mm/year in the Morais Massif).

Spectra Decomposition and Peak Matching

The results obtained with the methods of Spectra Decomposition and Peak Matching are summarized in Figure 7. Cells filled with patterns mark orientation classes corresponding to anomalous positive z-scores ($Z > 1$) in the three individual spectra. Dots were used for ZFL (fracture-length spectrum), squares for ZI (intrinsic properties), and horizontal lines for ZSF (stress field). Superposition between patterns occurred in two cells (orientation classes N20ºE and N40ºE in the SGC), in which cases we selected the pattern corresponding to the highest Z value. Bullets and circles represent major ($ZT > 1$) and minor ($0 < ZT < 1$) peaks in the standardized total spectra. While all major ZT peaks except one fall over filled cells (they are of the single-parameter type), minor peaks are placed preferably (9 in 14) in the white cells (multiple-parameter type). In the granites and SGC, major ZT peaks are all under to the fracture-length or intrinsic-density spectra, in the OTC they appear under the influence of the stress-field spectrum, and in the UATC are distributed under all three individual spectra.

As mentioned, the major ZFL peaks (dotted cells in Figure 7) arise whenever large-scale normal faults are locally controlling the spring distribution through genetically related fractures. In the granites and SGC, it is believed that the ZFL peaks striking N30º–40ºE and

N50º–60ºW appear because the Pinhão River Basin is located close to the Vila Real Fault and important NW-SE trending shear zones. In the UATC, appearance of a N80ºE ZFL peak is promoted probably by the Morais Fault. It is striking, however, that apparently the Vilariça Fault is not influencing the association between springs and fractures in the Morais Massif (no dots appear in the OTC or UATC cells), although the fault is just a few kilometers from the NW border of the Massif (see the locations of tectonic structures in Figure 1).

CONCLUSIONS

As demonstrated by Cross-Tabulation Analysis, the distribution of springs by fracture-orientation classes depends on the geological environment under study. With the method of Spectral Determination, it was possible to predict that the maximum number of springs per kilometer of fracture (intrinsic density) varies widely (0-12), depending on the fracture type, deformational regime, and fracture age. The methods of Spectra Decomposition and Peak Matching showed that, in general, the highest spring frequencies occur where groundwater flow is influenced by a single structural parameter (fracture length, intrinsic density, or the angle between the fracture strike and the present-day stress-field orientation), whereas the lowest ones are mostly of the multiple-parameter type, i.e. result from small groundwater contributions of more than one structural parameter.

ACKNOWLEDGEMENTS

Two anonymous reviewers are thanked for their comments and suggestions. They were of great help in improving an earlier version of this paper. The managing editor, Robert Schneider, is thanked for the linguistic advice.

REFERENCES

Alencoão AMP (1998) Os Recursos hídricos na bacia hidrográfica do rio Pinhão [The water resources in the hydrographic basin of the Pinhão river]. PhD thesis, University of Trás-os-Montes e Alto Douro, Vila Real, Portugal, 331p.

Bryan K (1919) Classification of springs. Jour. Geology, 27:522-561.

Diez Balda MA and Vegas R (1992) La estrutura del dominio de los pliegues verticales de la Zona Centro Iberica [The structure of the vertical folds domain of the Central Iberian Zone]. In: Gutiérrez Marco JG, Saavedra J and Rábano I (eds) Paleozoico Inferior de Ibero-America, University of Extremadura, Madrid, Spain, pp. 523-534.

Davis SN and DeWiest RJM (1991) Hydrogeology. Krieger Publishing Company, Malabar, Florida, USA, 463p.

Fedeli B and Castillo A (1997) Different kinds of morphogenetic springs in the upper Dilar valley (Sierra Nevada, Granada, Spain). In: Yélamos JG and Villarroya F (eds) Hydrogeology of hard rocks, some experiences from Iberian Peninsula and Bohemian Massif, Faster, Madrid, Spain, pp 159-167

Genter A (1990) Geothermie des roches chaudes séches, le granite de Soultz-Sous-Forêts (Bas-Rhin, France). Fracturation naturelle, alterations hydrothermales et interation eau-roche [Geothermy of the hot and dry rocks, the . Soultz-Sous-Forêts granite (Bas-Rhin, France). Natural fracturation, hydrothermal alterations and water-rock interactions]. Document du BRGM, 185, 85-94.

Jobson JD (1991) Applied multivariate data analysis, volume 2 - Categorical and multivariate methods. Springer Verlag, New York, 731p.

Marques FG, Ribeiro A and Pereira E (1992) Tectonic evolution of the deep crust: Variscan reactivation by extension and thrusting of Precambrian basement in the Bragança and Morais massifs (Trás-os-Montes, NE Portugal). Geodynamica Acta, 5:135-151.

Marques FO, Ribeiro A and Munhá JM (1996) Geodynamic evolution of the Continental Allochthonous Terrane (CAT) of the Bragança Nappe Complex, NE Portugal. Tectonics, 15:747-762.

Martín G, Casas S, Suso JM and Molina MA (1997) Inventario de puntos de agua en rocas graníticas. Sistemática en la realización e interpretación de datos [Inventory of water sites in granitic rocks. Systematic creation and interpretation of data]. In: Yélamos JG and Villarroya F (eds) Hydrogeology of hard rocks, some experiences from Iberian Peninsula and Bohemian Massif, Faster, Madrid, Spain, pp 55-66.

Matos AV (1991) A geologia da região de Vila Real [The geology of the Vila Real region]. PhD thesis, University of Trás-os-Montes e Alto Douro, Vila Real, Portugal, 312p.

Pacheco FAL (2000) Hidrogeologia em maciços cristalinos fracturados (Chacim - Morais - Macedo de Cavaleiros): contribuição para a gestão integrada dos recursos hídricos da região [Hydrogeology in fractured crystalline massifs (Morais - Chacim - Macedo de Cavaleiros): a contribution for the integrated management of the regional water resources]. PhD thesis, University of Trás-os-Montes e Alto Douro, Vila Real, Portugal, 395p.

Pereira E, Ribeiro A and Meireles C (1993) Cizalhamentos hercínicos e controle das mineralizações de Sn e W, Au e U na Zona Centro Ibérica em Portugal [Hercynian shear faults and control of the Sn and W, Au and U ores in the Central Iberian Zone in Portugal]. Cuader, Lab. Xeol., De Laxe, 18:89-119.

Pinto MS, Casquet C, Ibarrola E, Corrétge LG and Ferreira MP (1987) Síntese geocronológica dos granitóides do Maciço Hespérico [Chronological synthesis of the granitoids in the Hesperic massif]. In: Bea F, Carmina A, Gonzalo JC, Plaza ML and Rodrigues JML (eds), Geologia de los granitóides e rocas associadas del Macizo Hespérico. Libro de Homenage a Garcia Figueirola LC, Rueda, Madrid, Spain, pp 69-86.

Portugal Ferreira MR and Pacheco FAL (1997) Groundwater in metamorphic rocks with systematic fractures: inhomogeneous systems. Acta Universitatis Wratislaviensis, 2052:33-45.

Ribeiro A (1974) Contribution à l'étude tectonique de Trás-os-Montes Oriental [Contribution to the study of East Trás-os-Montes tectonics]. Memórias dos Serviços Geológicos de Portugal, 24:1-177.

Ribeiro A, Pereira E and Dias R (1990) Structure in the NW of the Iberian Peninsula. In: Dallmeyer RD and Martinez E (eds) Pre-Mesozoic Geology of Iberia, Springer Verlag, New York, pp 220-236.

Ribeiro A, Cabral J, Baptista R and Matias L (1996) Stress pattern in Portugal mainland and the adjacent Atlantic region, West Iberia. Tectonics, 15:641-659.

Sousa MB (1982) Litostratigrafia e estrutura do Complexo Xisto-Grauváquico ante Ordovícico, Grupo do Douro (Nordeste de Portugal) [Lithostratigraphy and structure of the ante-Ordovician Schist and Greywacke Complex, Douro Group (Northeast Portugal)]. PhD thesis, University of Coimbra, Coimbra, Portugal, 222p.

Todd DK (1980) Groundwater hydrology. John Wiley & Sons, New York, 535p.

TABLE 1

Spatial (N_A) and linear (Nk) spring densities in the Pinhão River Basin (PRB) and Morais Massif (MM). Outcrop areas are in agreement with Figures 2a,b; lineament plus fracture lengths with Figures 3a,b; and spring frequencies with Figures 4a,b.

Lithological Unit		Outcrop Area (km^2)	Lineament plus Fracture Lengths L (km)	Spring Frequency N (L^0)	N_A (L^{-2})	Nk (L^{-1})
PRB	Granites	183.2	1023.9	696	3.8	0.7
	SGC	96.8	365.4	184	1.9	0.5
MM	Amphibolites	222.0	665.4	372	1.7	0.6
	Ultramafics	57.5	168.7	99	1.7	0.6
	Gneisses	37.4	86.2	48	1.3	0.6
	Micaschists	46.1	218.9	138	3.0	0.6

TABLE 2

Distribution of springs and lengths of lineaments/fractures per orientation classes and geological environments with markedly different deformational histories; fracture-orientation classes are in relation to the left limit of the fractures. Symbols: SGC - Schist and Greywacke Complex; OTC - Ophiolitic Thrust Complex; UTAC - Upper Allochthonous Thrust Complex; N.A. - Not attributed to any orientation class.

		Springs N_i (L^0)					Fractures L_i (km)				N_i/L_i (L^{-1})			
		Granites	SGC	OTC	UATC	Total	Granites	SGC	OTC	UATC	Granites	SGC	OTC	UATC
Orientation Class	EW	8	1	18	2	29	22.5	6.7	38.9	19.9	0.4	0.1	0.5	0.1
	N80ºW	14	7	30	12	63	21.8	22.2	68.8	11.2	0.6	0.3	0.4	1.1
	N70ºW	13	3	60	12	88	27.9	10.8	28.1	9.1	0.5	0.3	2.1	1.3
	N60ºW	36	6	27	7	76	87.3	21.7	50.5	28.7	0.4	0.3	0.5	0.2
	N50ºW	25	12	12	4	53	74.7	37.9	85.8	35.1	0.3	0.3	0.1	0.1
	N40ºW	15	7	26	9	57	37.8	29.6	69.9	5.9	0.4	0.2	0.4	1.5
	N30ºW	12	1	15	4	32	47.6	9.7	18.7	4.4	0.3	0.1	0.8	0.9
	N20ºW	17	1	14	4	36	53.8	6.8	25.0	3.7	0.3	0.1	0.6	1.1
	N10ºW	36	1	27	9	73	72.4	6.3	25.1	30.6	0.5	0.2	1.1	0.3
	NS	23	4	33	8	68	65.2	10.5	38.2	15.0	0.4	0.4	0.9	0.5
	N10ºE	24	2	25	3	54	42.5	3.4	23.6	3.3	0.6	0.6	1.1	0.9
	N20ºE	61	12	22	6	101	67.1	35.6	57.2	7.9	0.9	0.3	0.4	0.8
	N30ºE	57	14	20	18	109	133	66.4	71.3	17.6	0.4	0.2	0.3	1.0
	N40ºE	54	18	18	3	93	146.9	35.3	71.7	25.3	0.4	0.5	0.3	0.1
	N50ºE	19	9	10	9	47	39.7	16.5	75.7	31.7	0.5	0.5	0.1	0.3
	N60ºE	14	6	14	4	38	30	9.3	26.0	8.0	0.5	0.6	0.5	0.5
	N70ºE	17	5	12	22	56	25.7	14.7	28.3	15.4	0.7	0.3	0.4	1.4
	N80ºE	16	7	41	27	91	28	22	31.6	32.5	0.6	0.3	1.3	0.8
N.A.		235	68	47	23	373								
Total		696	184	471	186	1537	1023.9	365.4	834.1	305.0				

TABLE 3

Results of the Spectral Determination procedure; fracture-orientation classes are in relation to the left limit of the fractures. Geological environments: SGC - Schist and Greywacke Complex; OTC - Ophiolitic Thrust Complex; UTAC - Upper Allochthonous Thrust Complex. Symbols: θ_i - Angle between the i^{th} orientation class and S_{Hmax} (represented by the N75ºW direction); c_i - Intrinsic spring density (calculated by Equation 7a); F1, F2 and F3 - Deformation phases of the Hercynian orogeny; L, C and D/Da - Fold generated fractures, respectively longitudinal, cross, and diagonal (conjugate pair); DF, DFF, and FF - Ductile, ductile/fragile, and fragile faults.

Orientation Class	θ_i	Granites				SGC					OTC					UATC				
		c_i (L^{-1})	Syn-F3	Late-F3	Post-F3	c_i (L^{-1})	F1,F2	Syn-F3	Late-F3	Post-F3	c_i (L^{-1})	F1		Syn-F3	Late- to Post-F3	c_i (L^{-1})	F1		Syn-F3	Late- to Post-F3
												Body of the Complex	Thrust Surface				Body of the Complex	Thrust Surface		
EW	15	0.4				0.2					0.5		C	DF		0.1			DF	
N80ºW	5	0.6				0.3					0.4			DF		1.1			DF,D	
N70ºW	5	0.5				0.3					2.1			D		1.3				
N60ºW	15	0.4	DF			0.3		DF			0.6		Da	DF		0.3	L		DF	
N50ºW	25	0.4	DF			0.3	L	DF			0.2	L		DF		0.1			DF,C	
N40ºW	35	0.5	DF			0.3		DF			0.5			C,DF		1.9		D	DF	
N30ºW	45	0.4				0.1					1.1					1.3				
N20ºW	55	0.6				0.3					1.0					1.9			Da	
N10ºW	65	1.2		DFF		0.4			DFF		2.6			Da		0.7		C		
NS	75	1.4		DFF		1.5			DFF		3.3		L		FF	2.1	D			FF
N10ºE	85	6.5			FF	6.7	D			FF	12.2	D			FF	10.4				FF
N20ºE	85	10.4			FF	3.9				FF	4.4				FF	8.7		Da		FF
N30ºE	75	1.7		DFF		0.8			DFF		1.1				FF	4.0	C			FF
N40ºE	65	0.9		DFF		1.2	C		DFF		0.6	C				0.3			L	
N50ºE	55	0.8		DFF		1.0			DFF		0.2			L		0.5				
N60ºE	45	0.7	DF			0.9		DF			0.8		D			0.7	Da			
N70ºE	35	0.8	DF			0.4	Da	DF			0.5	Da				1.7				
N80ºE	25	0.6	DF			0.4		DF			1.4			DF		0.9		L	DF	

TABLE 4

Intrinsic spring densities assembled according to fracture ages, deformational regimes, and fracture types.

Hercynian Phase (Age Decreasing Downwards)	Deformation Regime	Fracture Type		
		Tensional Fracture	Shear Fracture	
		Longitudinal, Cross	Diagonal Fracture	Fault
		Intrinsic Density, c_i (L^{-1})		
F1	Fragile	0–1	0–1	
Syn-F3	Ductile	0–1	1–3	0–2
Late-F3	Ductile/Fragile			0–4
Post-F3	Fragile			4–12

FIGURE CAPTIONS

Fig. 1: Geological framework of the study area. Symbols: PRB - Pinhão River Basin; MM - Morais Massif; VRF - Vila Real Fault; VF - Vilariça Fault; MF - Morais Fault; (1) - Autochthon (Schist and Greywacke Complex - SGC) and Parautochthon; (2) - Lower Allochthonous Thrust Complex (LATC); (3) - Ophiolitic Thrust Complex (OTC); (4) - Upper Allochthonous Thrust Complex (UATC); (5) - Granite; (6) - Thrust FAULT; (7) - Probable thrust fault; (8) - Ductile shear zone; (9) - Fragile fault.

Fig. 2a: Simplified geological map of the Pinhão River Basin. Source: Alencoão (1998); based on a combination of original drawings by Sousa (1982) and Matos (1991).

Fig. 2b: Simplified geological map of the Morais Massif. Symbols: OTC - Ophiolitic Thrust Complex; UATC - Upper Allochthonous Thrust Complex; OTC_A - Lower ophiolite; OTC_B - Upper ophiolite; 1 - Serpentinites, flaser gabbros, and sheeted dyke complex; 2 - Amphibolites; 3 - Serpentinites and flaser gabbros; 4 - Serpentinites, gabbros, flaser gabbros, and sheeted dyke complex; 5 - Granulites and peridotites; 6 - Lagoa augengneisses; 7 - Lagoa micaschists. Source: Marques *et al*. (1992); original drawing by Ribeiro *et al*. (1990).

Fig. 3: (a) Structural map of the Pinhão River Basin (Alencoão, 1998); (b) Map of lineaments of the Morais Massif (Pacheco, 2000), based on interpretation of aerial photographs.

Fig. 4: Spring densities: (a) Pinhão River Basin (Alencoão, 1998); (b) Morais Massif (Pacheco, 2000).

Fig. 5: Flowchart illustrating the method of Spectra Decomposition.

Fig. 6a: Total spectra drawn for the granites and SGC (Pinhão River Basin); fracture-orientation classes are in relation to the left limit of the fractures; conditional probabilities (Equation 3) replaced spring frequencies so that spectra could be easily compared.

Fig. 6b: Total spectra drawn for the OTC and UATC (Pinhão River Basin); fracture-orientation classes are in relation to the left limit of the fractures; conditional probabilities (Equation 3) replaced spring frequencies so that spectra could be easily compared.

Fig. 7: Results of the Peak Matching procedure; fracture-orientation classes are in relation to the left limit of the fractures.

FIGURE 1

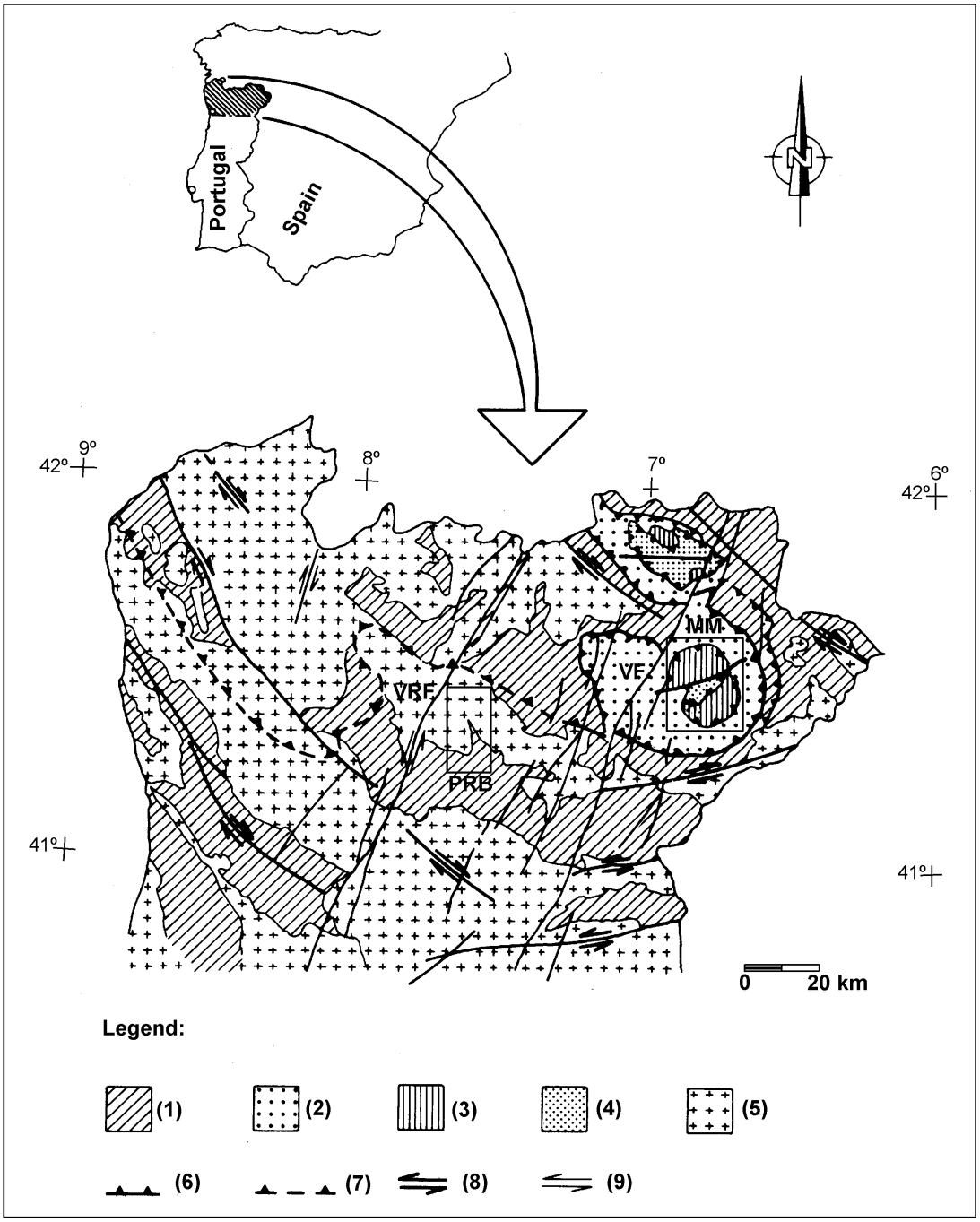
Portugal
Spain
N
9º
42º
8º
7º
6º
42º
41º
41º
MM
VF
VRF
PRB
0
20 km
Legend:
(1)
(2)
(3)
(4)
(5)
(6)
(7)
(8)
(9)

FIGURE 2a

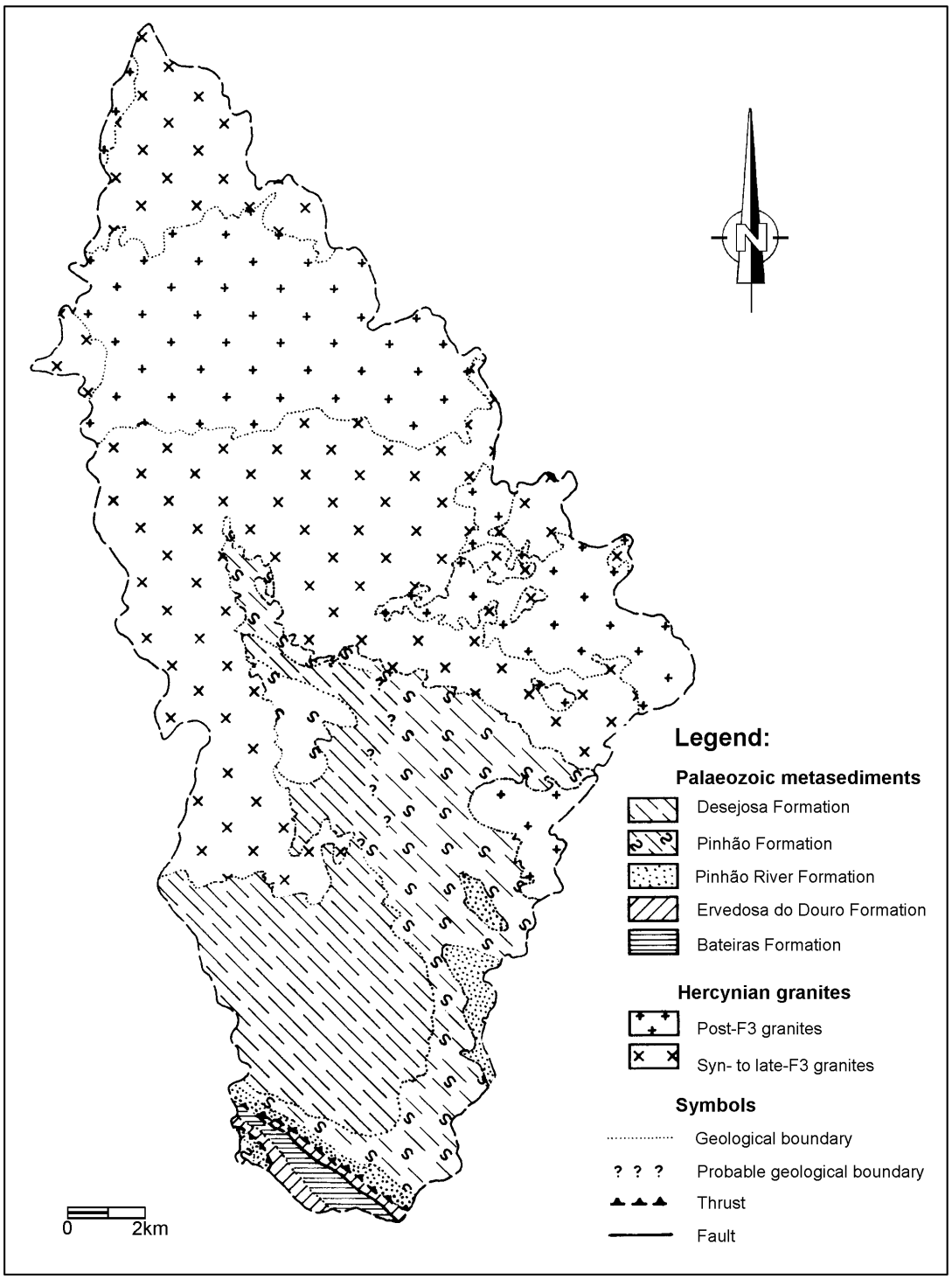
N
Legend:
Palaeozoic metasediments
Desejosa Formation
Pinhão Formation
Pinhão River Formation
Ervedosa do Douro Formation
Bateiras Formation
Hercynian granites
Post-F3 granites
Syn- to late-F3 granites
Symbols
Geological boundary
Probable geological boundary
Thrust
Fault
0
2km

FIGURE 2b

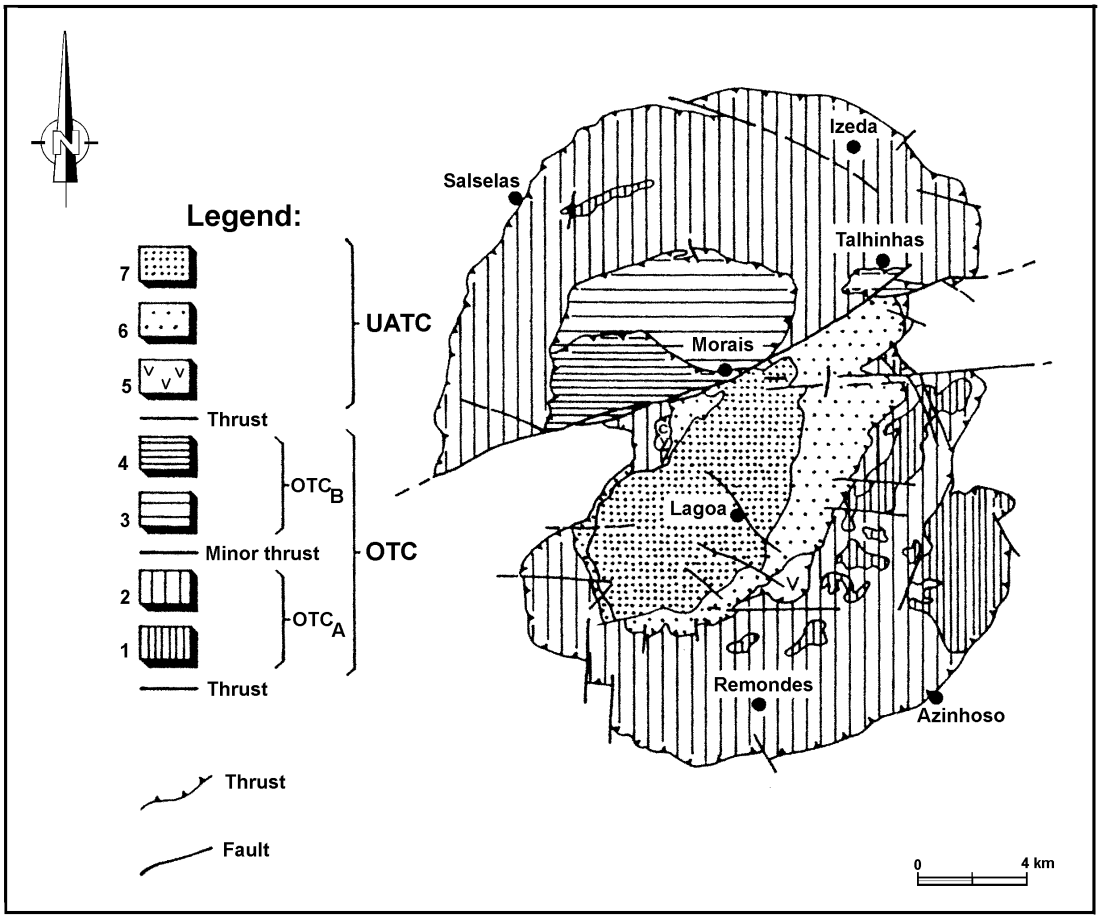
Legend:
7
6
5
UATC
Thrust
4
3
OTC$_B$
Minor thrust
OTC
2
1
OTC$_A$
Thrust
Thrust
Fault
Izeda
Salselas
Talhinhas
Morais
Lagoa
Remondes
Azinhoso
0
4 km

FIGURE 3

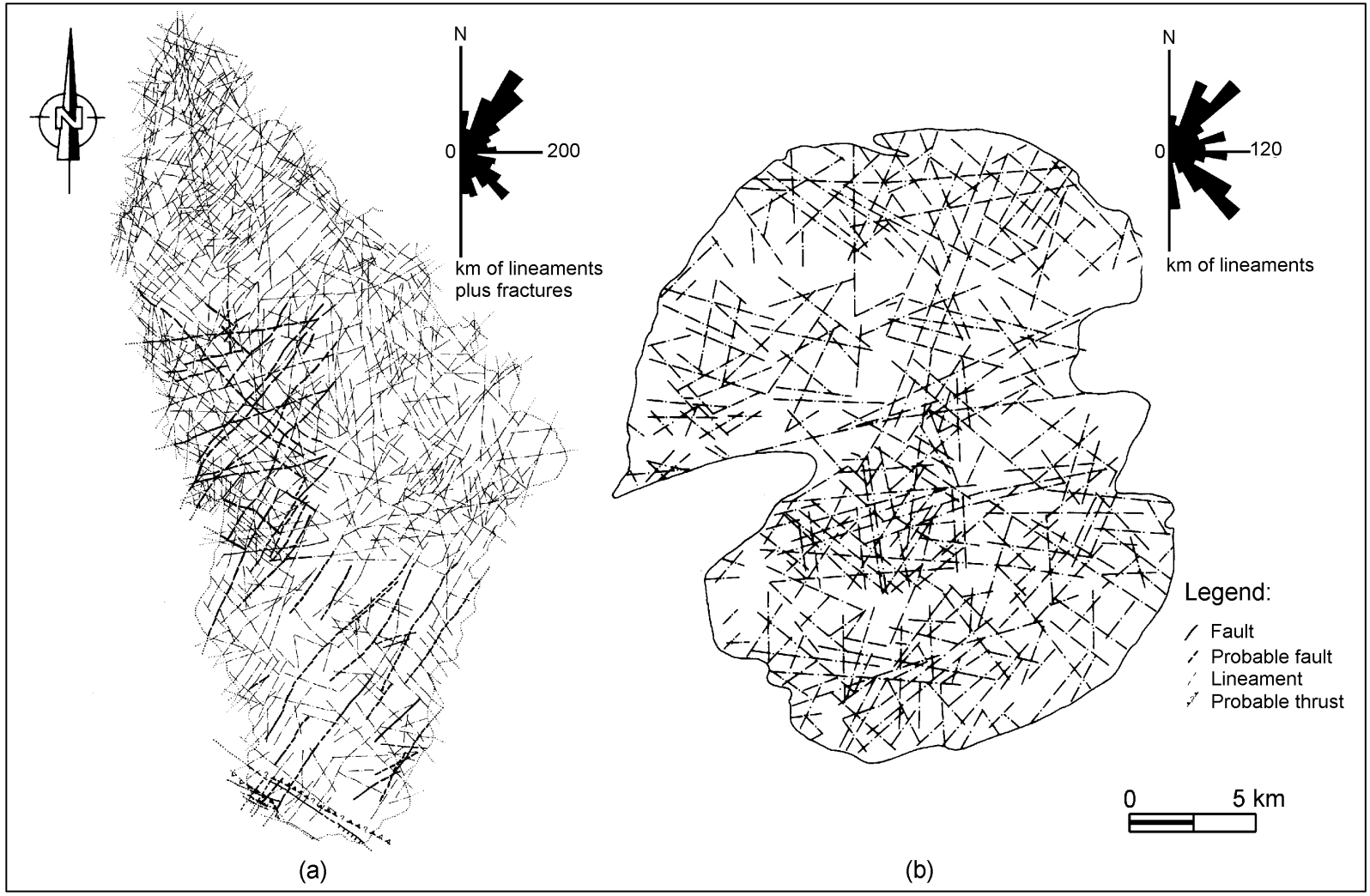
N
0
200
km of lineaments
plus fractures
(a)
N
0
120
km of lineaments
Legend:
Fault
Probable fault
Lineament
Probable thrust
0
5 km
(b)

FIGURE 4

FIGURE 5

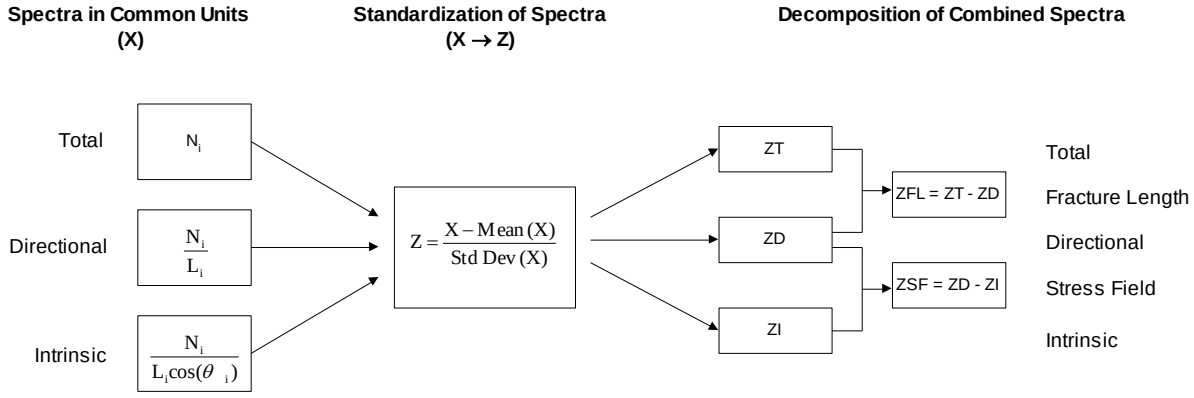
Spectra in Common Units
(X)
Standardization of Spectra
(X → Z)
Decomposition of Combined Spectra
Total
Directional
Intrinsic
N_i
$\frac{N_i}{L_i}$
$\frac{N_i}{L_i \cos(\theta_i)}$
$Z = \frac{X - Mean(X)}{Std\ Dev(X)}$
ZT
ZD
ZI
ZFL = ZT - ZD
ZSF = ZD - ZI
Total
Fracture Length
Directional
Stress Field
Intrinsic

FIGURE 6a

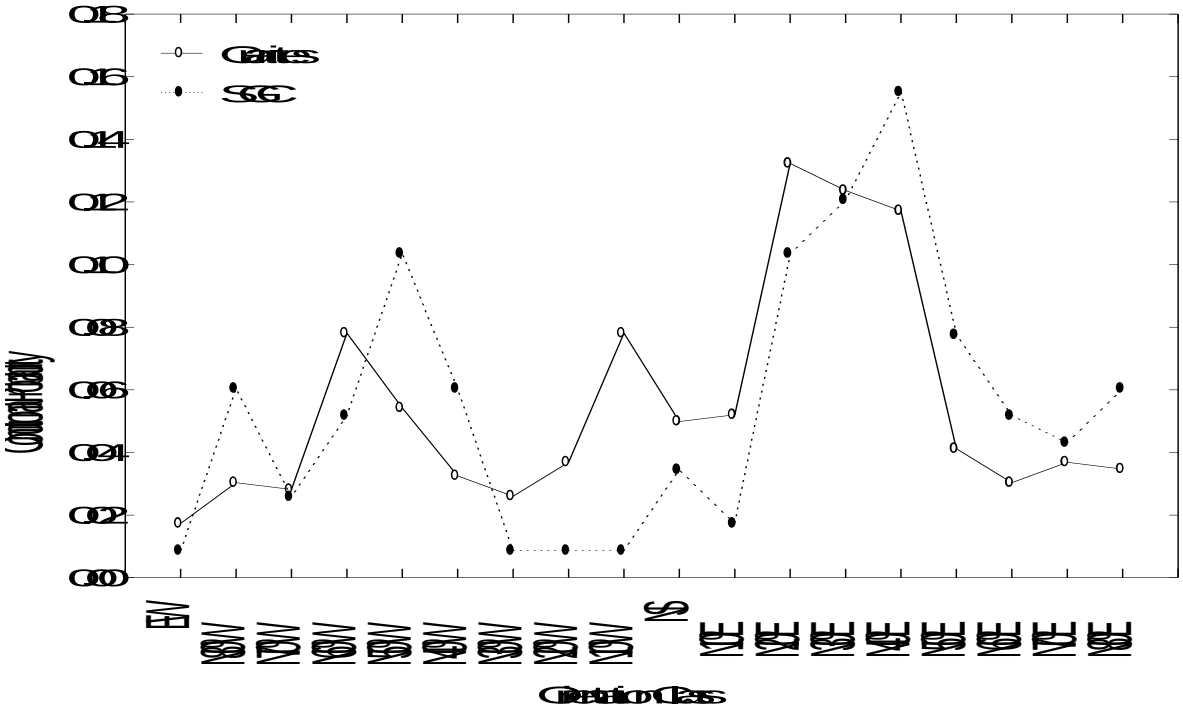

FIGURE 6b

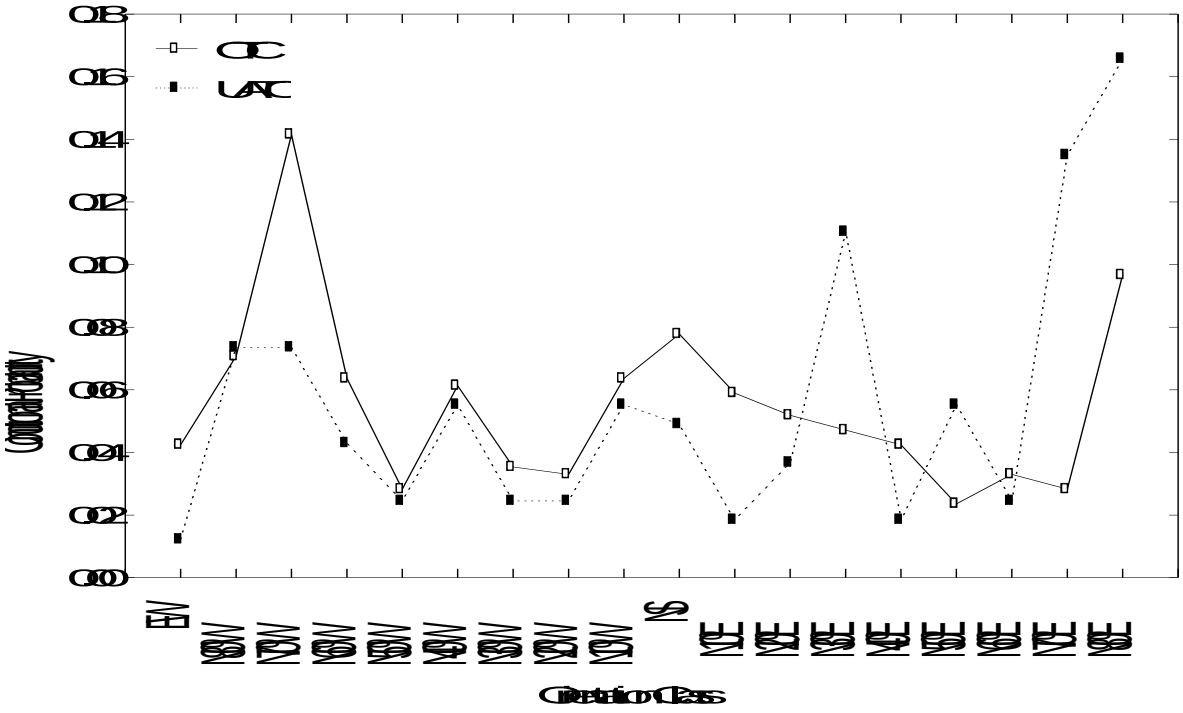

FIGURE 7

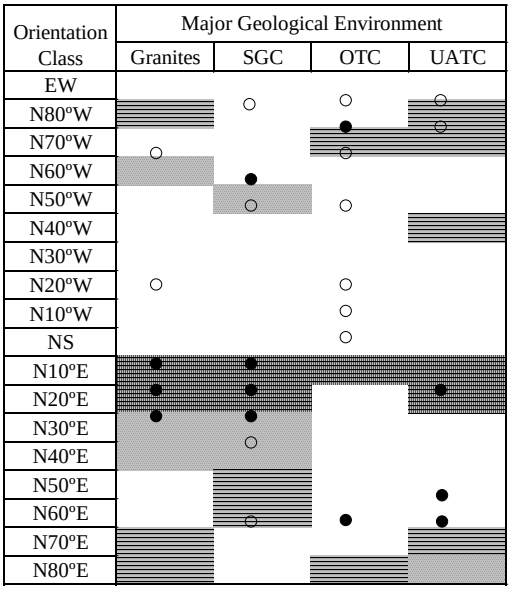

Legend

Pattern — Individual spectra determining spring occurrence

- Large-scale normal faults (ZFL>1)
- Genetic properties of fractures (ZI > 1)
- Parallelism with the stress field orientation (ZSF>1)
- A small contribution (0<Z<1) from one or more spectra

Total spectra (observed spring frequencies)

- ● Major peaks (ZT>1)
- ○ Minor peaks (0<ZT<1)